ISSN No:-2456-2165 https://doi.org/10.38124/ijisrt/26nov114

Thermal Balance and Recovery Potential of Shell Heat Losses from a Rotary Lime Kiln: Radiative–Convective Modelling, Exergy and Thermomechanical Constraints (Carrilu S.A., Kolwezi, DR Congo)

Lumpungu Mabeya Kasongo Deguy[1]; Mwaba Kalumba Raphaël[2]

[1]MSc Assistant, PhD Candidate, Institut Supérieur Des Techniques Appliquées De Kolwezi
[2]Department of Mechanical Engineering, Institut Supérieur Des Techniques Appliquées De Kolwezi (ISTA/Kolwezi), P.O. Box 299, Kolwezi, Lualaba, Democratic Republic of Congo.

Publication Date: 2026/11/23

Abstract: The rotary kiln of the second lime production line at Carrilu S.A. (Kolwezi, Democratic Republic of the Congo) releases heat into the surrounding workshop, which degrades working conditions and represents an energy loss. The source thesis quantified this resource as the sensible energy stored in the steel shell (34.2 GJ), a quantity that is not a power. This paper establishes the steady-state thermal balance of the shell from the 30 surface temperature readings reported in the thesis (mean 261.6 °C; standard deviation 33.8 K). The heat flux is computed with the Stefan–Boltzmann law and mixed-convection correlations (Churchill–Chu and Churchill–Bernstein). The shell (804 m²) loses 4.20 MW, 70% of which by radiation; the 90% Monte Carlo interval spans 3.80–4.60 MW, and the exergy content of the loss is 1.84 MW. The stored energy reported in the thesis corresponds to only 2.3 h of these losses. A recovery model based on concentric absorber panels, coupled with the thermal resistance of the refractory wall, shows that the recovered heat is weakly sensitive to the collector temperature (3.26 to 2.85 MW between 60 and 300 °C), whereas the shell temperature rises steeply. Under the constraint Ts ≤ 320 °C, the optimum collector temperature is about 158 °C. At this point, 3.13 MW are recovered, about 330 kWe can be generated by an organic Rankine cycle, and 0.23 MW of kiln losses are avoided. Raising 34 bar steam, as proposed in the thesis, would drive the shell to 358 °C.

Keywords: *Rotary Kiln; Shell Heat Loss; Thermal Radiation; Mixed Convection; Exergy; Waste Heat Recovery; Democratic Republic of the Congo.*

How to Cite: Lumpungu Mabeya Kasongo Deguy; Mwaba Kalumba Raphaël (2026) Thermal Balance and Recovery Potential of Shell Heat Losses from a Rotary Lime Kiln: Radiative–Convective Modelling, Exergy and Thermomechanical Constraints (Carrilu S.A., Kolwezi, DR Congo). *International Journal of Innovative Science and Research Technology*, 11(11), 1168-1175. https://doi.org/10.38124/ijisrt/26nov114

I. INTRODUCTION

Rotary kilns in cement and lime plants are among the most energy-intensive industrial units. Shell losses account for 3–25% of the heat input, depending on the process (Stojić et al., 2022), and their recovery, either for air preheating or for power generation, has been widely investigated (Kasaeian et al., 2025; Marenco-Porto et al., 2023). In the Democratic Republic of the Congo (DRC), the incentive is twofold. First, only about 1,800 MW of the 2,600 MW of installed capacity on the national grid are actually available, and mining companies in Katanga and Lualaba resort to costly diesel back-up when supply fails (Cussaguet, 2025). Second, the heat radiated by kilns degrades working conditions in the surrounding workshops.

The Carrilu S.A. plant in Kolwezi produces cement and lime from a limestone deposit of more than 550 million tonnes. The rotary kiln of its second lime production line (diameter 4 m, effective length 64 m) has a shell temperature exceeding 240 °C. The source thesis (Mwaba Kalumba, 2024) proposed converting this heat into electricity with a 34 bar Rankine cycle in order to supply the 4.5 MW plant load. The approach, however, contains an error of principle: the "available heat" is computed as the sensible energy of the steel shell, $Qd = m\ cp\ \Delta T = 34.2$ GJ. This stored energy is not a power and provides no information on the heat rate the kiln can deliver continuously. The thesis then requires 18.75 MW from the boiler without verifying that such a heat rate exists.

ISSN No:-2456-2165 https://doi.org/10.38124/ijisrt/26nov114

This paper revisits the problem on a rigorous heat-transfer basis. It has four objectives:

- To compute, from the measured temperatures, the steady-state heat loss rate of the shell, separating radiation and convection, with an uncertainty estimate;
- To assess the thermodynamic quality of this heat through its exergy;
- To clarify the relationship between the stored energy computed in the thesis and the power actually available;
- To model a recovery device and determine the collector temperature that maximises the convertible electric power under a shell temperature constraint.

Power conversion itself is analysed in a companion paper.

II. LITERATURE REVIEW

- Rotary kiln shell losses. Stojić et al. (2022) report that shell losses range from 3 to 25% of the heat input and analyse an annular recuperator able to capture the equivalent of the bare-kiln loss; rotational eccentricity of the shell is the most influential parameter. For a 4.6 m × 68 m cement kiln, Fierro et al. (2021) obtain an uninsulated shell temperature of about 375 °C, with 83% of the heat flow transferred by radiation at the hottest location. A full annulus of absorber panels would recover 4.98 MW, with a maximum absorber temperature of 240 °C.
- Power conversion. Recent reviews by Kasaeian et al. (2025) and Marenco-Porto et al. (2023) compare steam Rankine cycles, organic Rankine cycles (ORC), the Kalina cycle, supercritical CO_2 cycles and thermoelectric generators for cement plants. Mahmoud et al. (2022) evaluate a Kalina cycle fed jointly by the kiln shell, the preheater and the clinker cooler of a cement plant, obtaining 7.35 MW net for the combined configuration. Fierro et al. (2021) couple shell panels with a recuperated cyclopentane ORC, delivering 864 kWe net at a thermal efficiency of 17.35%.
- Analytical tools. Natural and forced convection correlations for horizontal cylinders and radiative exchange between grey surfaces are taken from Lienhard and Lienhard (2024). Exergy and Carnot efficiency follow Çengel et al. (2024).
- Research gap. To the authors' knowledge, no published work addresses a lime kiln in Central Africa on the basis of field measurements. Moreover, the cited studies impose the collector temperature. The present paper shows that, for a shell fed by conduction through the refractory lining, the shell temperature becomes the binding design constraint.

III. MATERIALS AND METHODS

➢ *Kiln and Measurements*

The kiln is a steel shell of diameter D = 4 m, effective length L = 64 m and thickness e = 50 mm, lined with refractory bricks. It is fired with pulverised coal and fuel oil; the calcination temperature reaches about 1,100 °C. The outer surface area is $A = \pi DL = 804$ m².

The thesis reports 30 surface temperature readings taken at 10 points along the shell (T1 to T10) in the morning, at noon and at night (Mwaba Kalumba, 2024). The overall mean is 261.6 °C, the standard deviation 33.8 K and the 95% confidence interval of the mean ±12.1 K. The period means are 259.7 °C (morning), 279.0 °C (noon) and 246.1 °C (night). The night reading of 116.7 °C at point T10 is atypical; excluding it would raise the mean to 266.6 °C. It was retained because no evidence justifies discarding it. Figure 1 shows the axial profile.

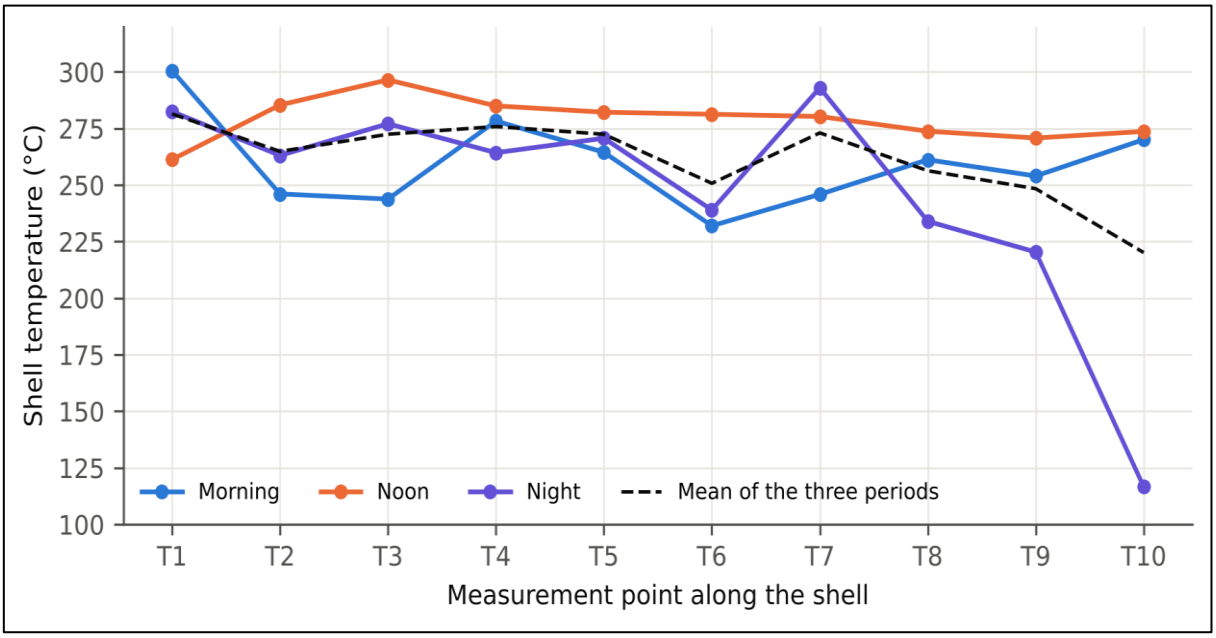


Fig 1 Shell Temperatures at the Ten Measurement Points by Period of the Day. Data: Mwaba Kalumba (2024).

ISSN No:-2456-2165 https://doi.org/10.38124/ijisrt/26nov114

➢ *Assumptions*

The ambient temperature is taken as 26.6 °C, the value used in the thesis. The emissivity of the oxidised steel shell is set at ε = 0.85, the air velocity at 2 m/s, and the effective inner temperature (gas and charge) at Tg = 1,100 °C. The shell is divided into ten zones of 80.4 m², each represented by its measurement point. Air properties are evaluated at the film temperature. All computations were performed in Python (NumPy, SciPy).

IV. THERMAL FORMULATION

➢ *Conduction Through the Kiln Wall*

Heat flows successively through the refractory lining and the steel shell. At steady state, Fourier's law applied to a cylindrical layer of radii r_i and r_o and conductivity λ gives the conduction resistance:

$$\Phi = \frac{2\pi\lambda L\,(T_i - T_o)}{\ln(r_o/r_i)}, R_{cyl} = \frac{\ln(r_o/r_i)}{2\pi\lambda L} \quad (1)$$

The resistances of the lining and the shell act in series. Since the actual lining thickness and conductivity are unknown, the wall is lumped into an equivalent areal resistance Rw (m²·K/W), identified from the measured state in Section 4.5.

➢ *Surface Radiation And Convection*

The shell, treated as a grey body, exchanges heat by radiation with surroundings much larger than itself, and by convection with ambient air:

$$q_r = \varepsilon\,\sigma(T_s^4 - T_\infty^4), q_c = h\,(T_s - T_\infty), \sigma = 5.670 \times 10^{-8}\ \mathrm{W\,m^{-2}\,K^{-4}} \quad (2)$$

The coefficient h results from mixed convection. Natural convection around a horizontal cylinder is described by the Churchill–Chu correlation, and forced convection in cross-flow by the Churchill–Bernstein correlation (Lienhard & Lienhard, 2024):

$$\overline{Nu}_N = \left\{0.60 + \frac{0.387\,Ra_D^{1/6}}{\left[1+(0.559/Pr)^{9/16}\right]^{8/27}}\right\}^2, Ra_D = \frac{g\,\beta\,(T_s - T_\infty)\,D^3}{\nu\,\alpha} \quad (3)$$

$$\overline{Nu}_F = 0.3 + \frac{0.62\,Re_D^{1/2}\,Pr^{1/3}}{[1+(0.4/Pr)^{2/3}]^{1/4}}\left[1 + \left(\frac{Re_D}{282\,000}\right)^{5/8}\right]^{4/5}, Re_D = \frac{U\,D}{\nu} \quad (4)$$

Both contributions are combined by the usual mixed-convection rule for assisting or transverse flows:

$$\overline{Nu} = \left(\overline{Nu}_N^3 + \overline{Nu}_F^3\right)^{1/3}, h = \frac{\overline{Nu}\,k}{D} \quad (5)$$

The total heat loss rate is the sum over the ten shell zones:

$$\dot{Q}_p = \sum_{i=1}^{10} A_i\left[q_r(T_{s,i}) + q_c(T_{s,i})\right], A_i = \frac{\pi D L}{10} \quad (6)$$

Because the flux is strongly non-linear in Ts, the sum (6) differs from the product of the area by the flux evaluated at the mean temperature; both values are compared in Section 5.1.

➢ *Exergy of the Heat Loss*

The thermodynamic quality of a heat flow released at temperature Ts to an environment at T0 is measured by its exergy, i.e. the maximum work recoverable by a Carnot engine:

$$\dot{E}x = \dot{Q}_p\left(1 - \frac{T_0}{T_s}\right) \quad (7)$$

➢ *Stored Energy Versus Power: Transient Behaviour*

The quantity computed in the thesis is the sensible energy of the steel, Qd = m cp (Ts − T0), with m = ρsteel A e. It would be released only once, if the shell cooled down to ambient temperature. The energy balance of a shell deprived of any heat input, treated as a lumped capacitance, reads:

$$m\,c_p\,\frac{dT_s}{dt} = -A[q_r(T_s) + q_c(T_s)], \tau = \frac{m\,c_p}{h_{eq}\,A}, h_{eq} = \frac{q_r + q_c}{T_s - T_\infty} \quad (8)$$

The time constant τ indicates how long the steel alone could sustain the losses.

➢ *Recovery Model with Concentric Absorber Panels*

The device considered surrounds a fraction φ = 0.8 of the shell length (riding rings and girth gear excluded) with absorber panels located 0.5 m from the surface (Dc = 5 m). The panels carry a heat-transfer fluid at temperature Tc and are insulated on their outer face (Figure 2).

ISSN No:-2456-2165 https://doi.org/10.38124/ijisrt/26nov114

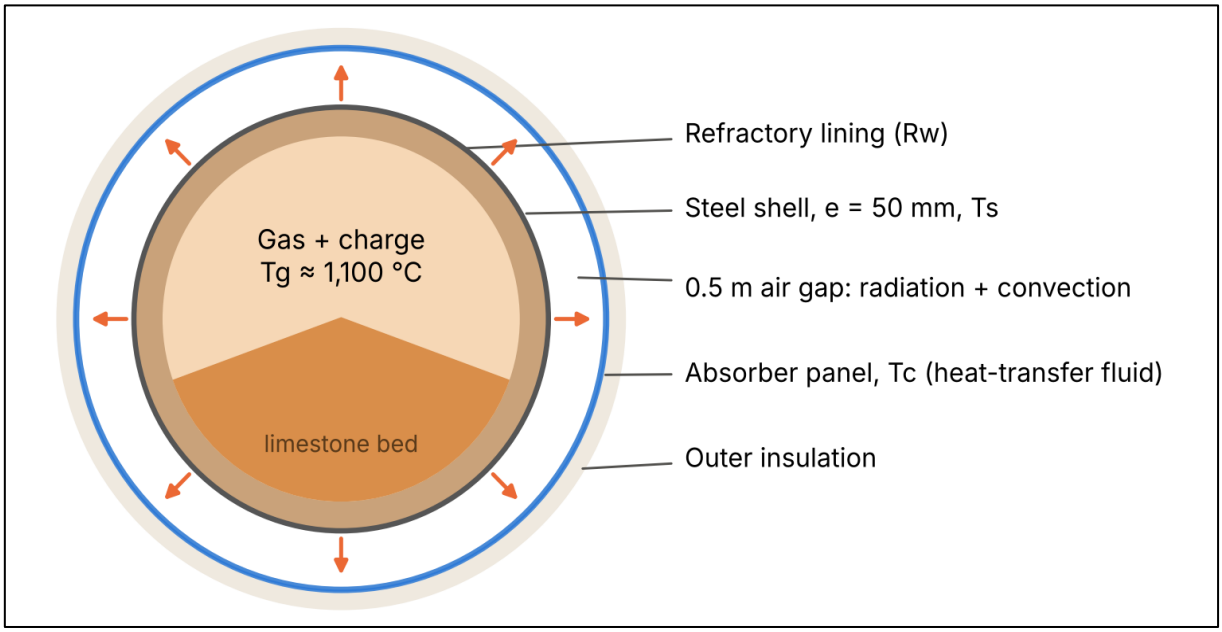


Fig 2 Schematic Cross-Section of the Kiln and the Concentric Collector.

The kiln wall is represented by an areal resistance Rw between the inner temperature Tg and the shell. It is identified zone by zone from the current state, in which all the conducted heat is lost at the surface:

$$R_{w,i} = \frac{T_g - T_{s0,i}}{q_{0,i}}, q_{0,i} = q_r(T_{s0,i}) + q_c(T_{s0,i}) \quad (9)$$

Exchange between the shell (εs = 0.85) and the panel (εc = 0.92, black coating) is that between two grey concentric cylinders, supplemented by convection in the air gap (hg = 5 W/m²·K):

$$q_{sc} = \frac{\sigma(T_s^4 - T_c^4)}{\frac{1}{\varepsilon_s} + \frac{D}{D_c}\left(\frac{1}{\varepsilon_c} - 1\right)} + h_g\,(T_s - T_c) \quad (10)$$

For each covered zone, the new shell temperature Ts,i is the root of the shell energy balance, solved by Brent's method:

$$\frac{T_g - T_{s,i}}{R_{w,i}} = q_{sc}(T_{s,i}, T_c) \quad (11)$$

The recovered heat and the change in heat extracted from the kiln relative to the current state follow:

$$\dot{Q}_{rec} = \varphi \sum_i A_i \frac{T_g - T_{s,i}}{R_{w,i}}, \Delta\dot{Q}_{kiln} = \varphi \sum_i A_i \left(\frac{T_g - T_{s,i}}{R_{w,i}} - q_{0,i}\right) \quad (12)$$

A negative ΔQ_kiln means that the collector acts as partial insulation: the kiln loses less heat than at present, which reduces its fuel consumption.

➢ *Convertible Electric Power and Optimisation*

The electric power is estimated by applying an overall second-law efficiency ηII to the Carnot efficiency. The latter is evaluated between the mean heat-addition temperature Tm ≈ Tc − 15 K and an air-cooled condenser at 45 °C:

$$P_e(T_c) = \dot{Q}_{rec}(T_c)\ \eta_{II}\left(1 - \frac{T_{cond}}{T_m}\right), \eta_{II} = 0.45 \quad (13)$$

The value ηII = 0.45 includes the generator and auxiliaries. It is consistent with the ORC of Fierro et al. (2021), whose 17.35% efficiency at a 240 °C absorber temperature corresponds to about 0.48 times the relevant Carnot efficiency. The collector temperature is selected by solving:

$$T_c^* = \underset{T_c}{\operatorname{argmax}}\ P_e(T_c) \text{ subject to } \max_i T_{s,i} \le T_{lim}, T_{lim} = 320\ °C \quad (14)$$

The 320 °C limit on the mean shell temperature is deliberately conservative. It remains below the levels at which operators monitor hot spots and lining degradation, and it limits differential expansion between the shell and the riding rings. It must be validated with the kiln manufacturer.

V. RESULTS

➢ *Shell Heat Loss*

At the mean temperature of 261.6 °C, the Rayleigh number is 3.2×10^{11} and the Reynolds number 2.9×10^5. The Nusselt numbers are 736 for natural convection and 453 for forced convection, giving 790 for mixed convection and h = 6.7 W/m²·K. The radiative flux reaches 3,552 W/m² and the convective flux 1,582 W/m², i.e. 5.13 kW/m² in total, and the overall equivalent heat transfer coefficient is 21.8 W/m²·K. Figure 3 shows the increase of the flux with temperature: radiation clearly dominates above 150 °C.

ISSN No:-2456-2165 https://doi.org/10.38124/ijisrt/26nov114

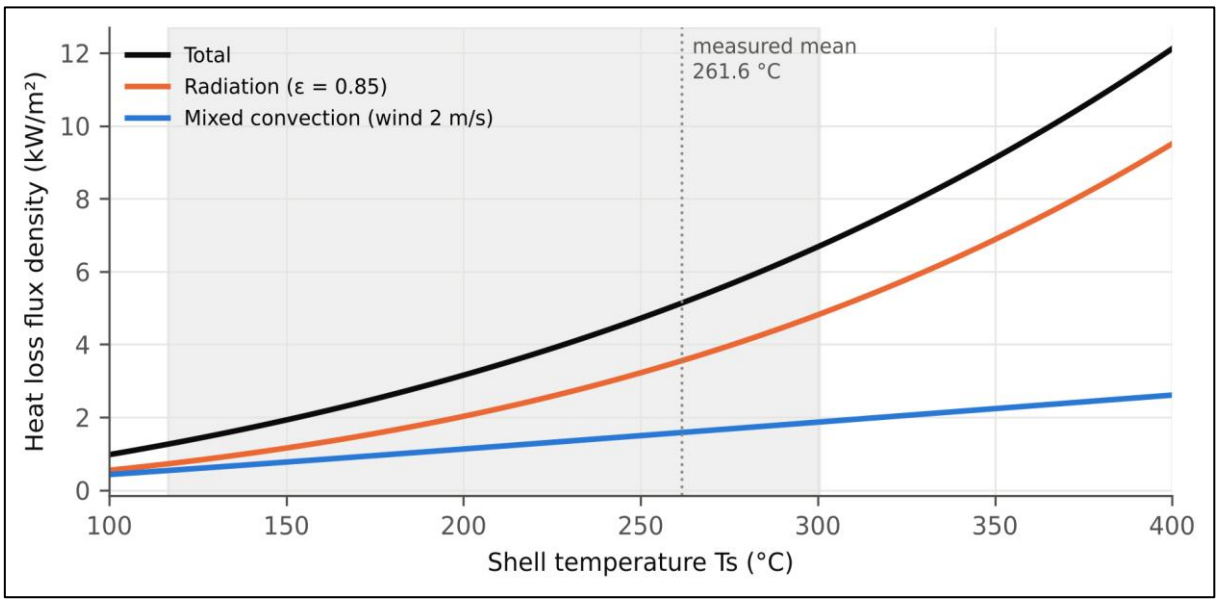


Fig 3 Radiative, Mixed-Convective and Total Heat Loss Flux Densities as Functions of Shell Temperature, Eqs. (2)–(5). Shaded Area: Range of Measured Temperatures.

Table 1 summarises the losses. According to Eq. (6), the shell loses 4.20 MW on a daily average, 69.7% of it by radiation. A calculation based on the mean temperature alone gives 4.13 MW: ignoring the temperature spread underestimates the losses by 1.6%. Losses peak at noon (4.67 MW), consistent with the higher temperatures recorded in that period.

Table 1 Shell Heat Losses by Measurement Period.

Period	Mean temperature (°C)	Heat loss rate (MW)
Morning	259.7	4.10
Noon	279.0	4.67
Night	246.1	3.82
Daily mean	261.6	4.20

Uncertainty was estimated with 5,000 Monte Carlo draws. Emissivity follows a uniform distribution between 0.75 and 0.92, wind speed a uniform distribution between 0.5 and 4 m/s, and the temperature measurement error a normal distribution with a standard deviation of 5 K. The median is 4.18 MW and the 90% interval spans 3.80–4.60 MW (Figure 4). Emissivity is the dominant source of uncertainty, followed by wind speed.

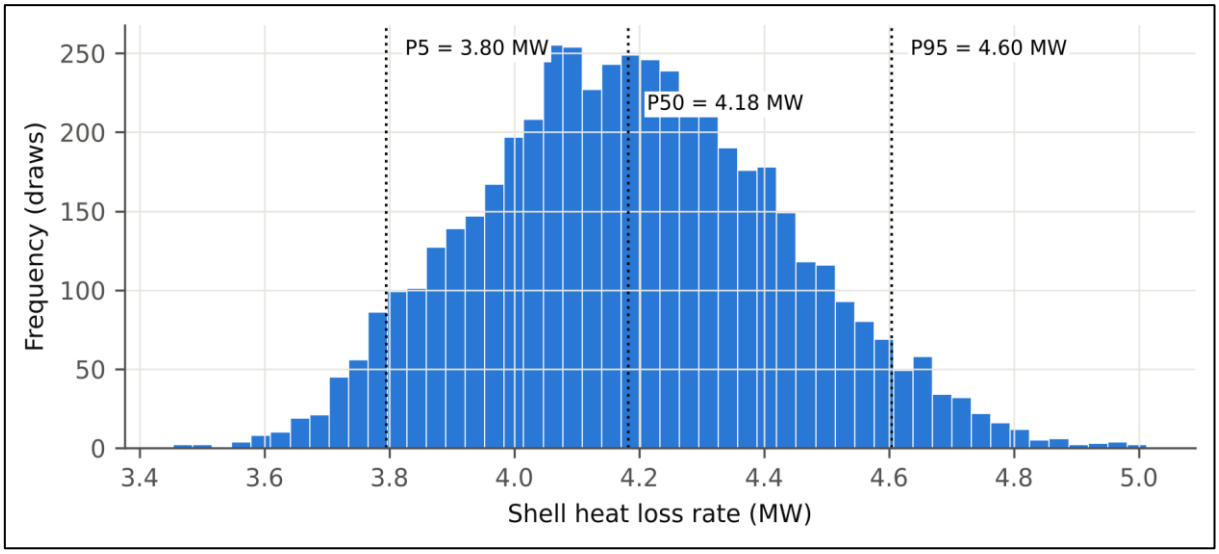


Fig 4 Distribution of the Shell Heat Loss Over 5,000 Monte Carlo Draws (Emissivity, Wind Speed, Measurement Error).

ISSN No:-2456-2165 https://doi.org/10.38124/ijisrt/26nov114

➢ *Exergy*

For Ts = 261.6 °C and T0 = 26.6 °C, the Carnot factor is 0.439. The exergy of the losses is therefore 1.84 MW, Eq. (7). No real cycle can generate more power from this heat released at the current shell temperature.

➢ *Stored Energy and Power*

The steel mass of the shell is 316 t and the sensible energy computed in the thesis, 34.2 GJ, is confirmed. However, it represents only 2.26 h of the current losses. The time constant of Eq. (8) is 8,270 s, i.e. 2.3 h. If the burner were shut down, the bare shell would cool below 150 °C in less than two hours (Figure 5). A power plant therefore cannot be sized on this energy: only the power sustained by combustion inside the kiln, about 4.2 MW, is continuously available. The 18.75 MW required from the boiler in the thesis exceeds this value by a factor of 4.5.

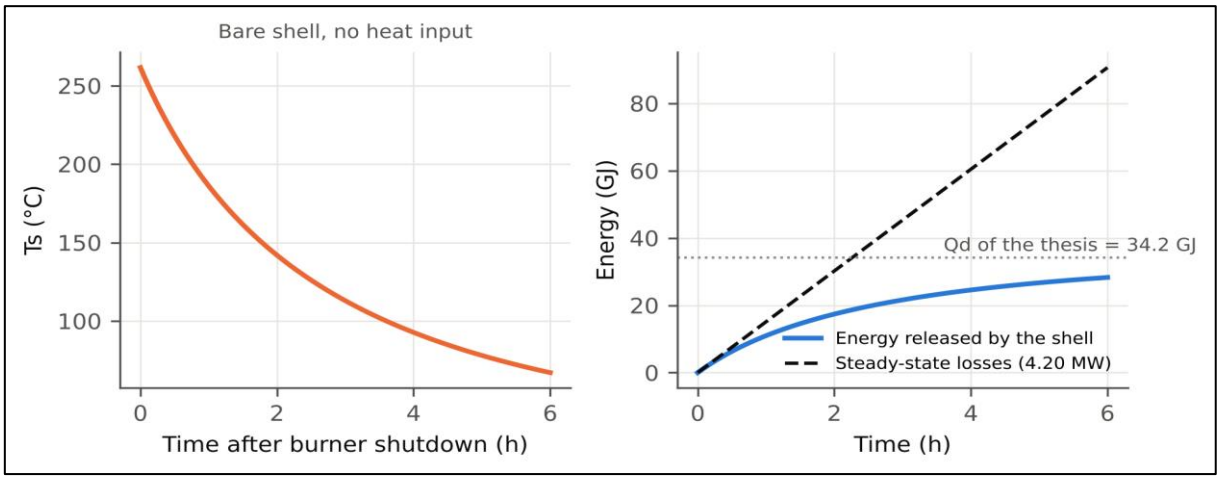


Fig 5 Left: Cooling of a Shell Deprived of Heat Input, Eq. (8). Right: Energy Released by the Steel Compared with the Energy Lost at Steady State.

➢ *Recovery Potential*

The wall resistance identified with Eq. (9) averages 0.163 m²·K/W. Figure 6 presents the results of the recovery model. The recovered heat decreases only slightly with collector temperature: 3.26 MW at 60 °C, 3.13 MW at 158 °C and 2.85 MW at 300 °C. This behaviour results from the large temperature difference between the kiln interior (1,100 °C) and the shell: the heat conducted through the lining changes little when the shell warms by a few tens of degrees. Conversely, because the collector is interposed between the shell and the atmosphere, the shell temperature rises rapidly with Tc: 287 °C for a collector at 60 °C, 316 °C at 150 °C, 358 °C at 241 °C and 391 °C at 300 °C.

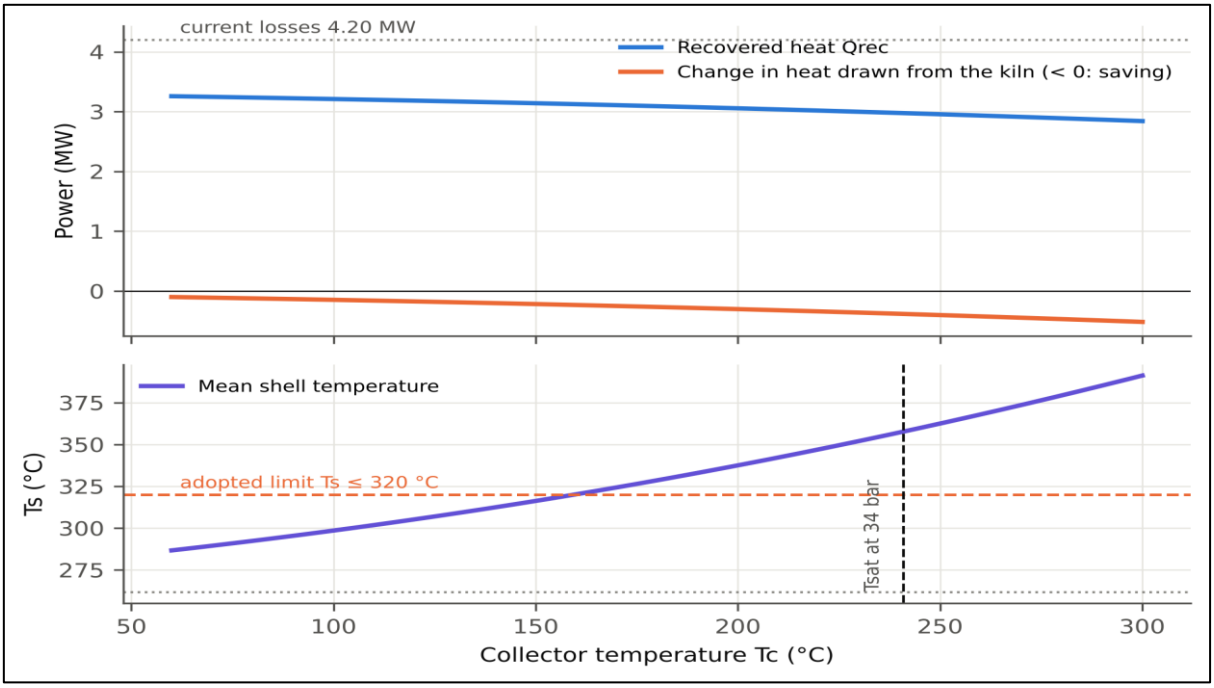


Fig 6 Top: Recovered Heat and Change in Heat Drawn from the Kiln, Eq. (12). Bottom: Mean Shell Temperature, Eq. (11), and the Adopted 320 °C Limit.

ISSN No:-2456-2165 https://doi.org/10.38124/ijisrt/26nov114

The change in heat drawn from the kiln is negative over the whole range, between −0.10 and −0.52 MW. The collector thus slightly reduces kiln losses, which yields a fuel saving independent of power generation.

➢ *Optimal Collector Temperature*

Figure 7 shows the convertible electric power. Without constraint, it increases monotonically with Tc and reaches 550 kWe at 300 °C, but at the cost of a shell at 391 °C. Under the constraint Ts ≤ 320 °C, the optimum of Eq. (14) is Tc* ≈ 158 °C. At this point, the recovered heat is 3.13 MW with a shell at 319 °C, the overall conversion efficiency 10.6%, the electric power about 330 kWe, and the avoided kiln losses 0.23 MW (Table 2).

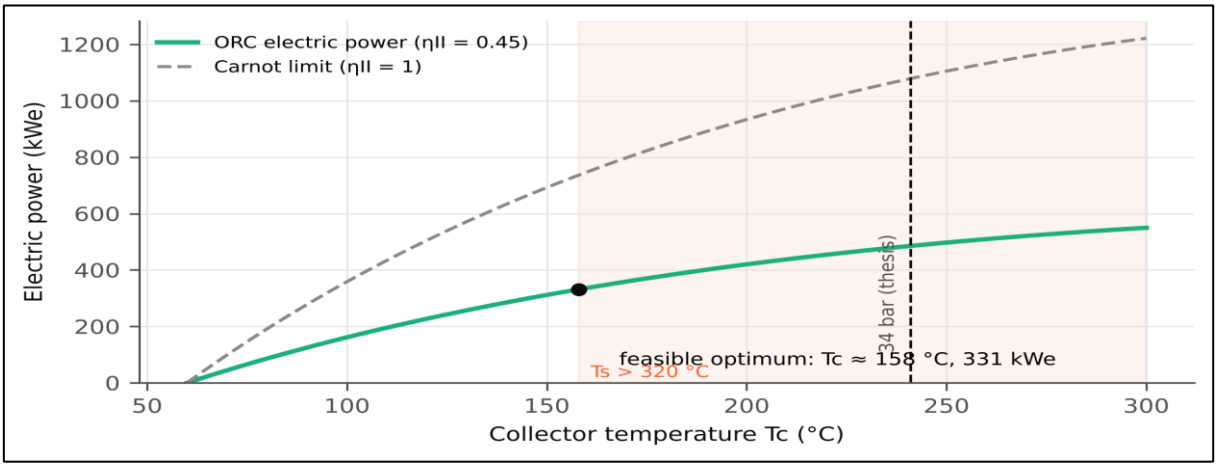


Fig 7 Convertible Electric Power According to Eq. (13) and the Carnot Limit. Orange Area: Shell Temperature above 320 °C.

Table 2 Characteristic Operating Points of the Recovery Device.

Collector temperature	Recovered heat (MW)	Shell temperature (°C)	Electric power (kWe)	Remark
60 °C	3.26	287	≈ 0	Water heating only
150 °C	3.14	316	312	Feasible
158 °C (optimum)	3.13	319	331	Ts = 320 °C limit reached
241 °C (34 bar, thesis)	2.97	358	485	Shell above limit
300 °C	2.85	391	550	Shell above limit

VI. DISCUSSION

➢ *Corrections Brought by the Analysis*

The first correction is conceptual: stored energy does not determine power. The 34.2 GJ reported in the thesis are correct as sensible energy, but they would sustain the losses for only 2.3 h. The relevant resource is the steady-state heat loss rate, 4.2 MW, whose exergy is only 1.8 MW. The second correction concerns orders of magnitude. The plant requires 4.5 MW of electricity, whereas even a reversible converter using all the available exergy could supply only 1.8 MW. A realistic system delivers about 0.33 MWe, i.e. 7% of the target load. The third correction is thermomechanical. Producing saturated steam at 34 bar requires a collector above 241 °C, which would raise the shell to about 358 °C. The device would then act as kiln insulation, with risks for the refractory lining and the riding rings.

➢ *Comparison with the Literature*

The results are consistent with those of Fierro et al. (2021). Their larger and hotter kiln (shell up to 375 °C) would offer at most 4.98 MW with a full annulus, against 3.1–3.3 MW here for 80% of the length of a cooler kiln. The radiative share, 70% on average here against 83% at the hottest location in their study, logically increases with temperature. As emphasised by Stojić et al. (2022), the actual collector geometry, particularly rotational eccentricity, governs the effectiveness; the concentric model used here is therefore an upper bound.

➢ *Benefit for Working Conditions*

The collector intercepts all the radiation emitted by the shell over the covered zones. The radiation received by operators is then that of the insulated outer face of the panels, close to ambient temperature. This improvement of the working environment, which motivated the thesis, is achieved whatever use is made of the recovered heat, including simple low-temperature water heating.

➢ *Limitations*

This study has four limitations. (1) Spot measurements taken over five days cannot replace a shell scanner; continuous monitoring would refine the axial profile and verify the 116.7 °C night reading. (2) The effective inner temperature and the wall resistance are identified rather than measured; an error in Tg shifts the curve of Figure 6 without changing its shape. (3) The model neglects kiln rotation and the uncovered riding-ring zones. (4) Power conversion is represented by an overall second-law efficiency; the companion paper analyses it cycle by cycle.

ISSN No:-2456-2165 https://doi.org/10.38124/ijisrt/26nov114

VII. CONCLUSIONS

The shell of the Carrilu S.A. rotary kiln loses 4.20 MW (90% interval 3.80–4.60 MW), 70% by radiation, with an exergy content of 1.84 MW. The stored energy of 34.2 GJ adopted in the thesis corresponds to only 2.3 h of these losses and cannot serve as a sizing basis. A concentric collector covering 80% of the shell would recover about 3.1 MW. Under the constraint Ts ≤ 320 °C, the optimal collector temperature is about 158 °C, for a convertible electric power of about 330 kWe and a 0.23 MW reduction in kiln losses. Supplying the 4.5 MW plant load is not achievable; a target of about 0.3 MWe, combined with a marked improvement in working conditions, is.

Further work should include an infrared shell-scanner campaign, the determination of the actual refractory lining, three-dimensional numerical modelling of the collector accounting for rotation, and a detailed analysis of the conversion cycle.

- Conflict of interest. The authors declare no conflict of interest.
- Data availability. The measured temperatures are reported in Mwaba Kalumba (2024); the calculation scripts are available from the authors upon request.

➢ *Nomenclature*

Symbol	Definition	Unit
A, A_i	Outer shell surface area; area of zone i	m²
D, Dc, L, e	Shell and collector diameters; length; steel thickness	m
Ts, Tc, Tg, T∞, T0	Shell, collector, effective inner, ambient and dead-state temperatures	°C or K
qr, qc, qsc	Radiative, convective and shell-to-collector heat flux densities	W/m²
h, hg, heq	Convective, air-gap and overall equivalent heat transfer coefficients	W/m²·K
ε, εs, εc	Emissivities (shell, collector)	—
σ	Stefan–Boltzmann constant	W/m²·K⁴
Nu, Ra, Re, Pr	Nusselt, Rayleigh, Reynolds and Prandtl numbers	—
k, ν, α, β	Thermal conductivity, kinematic viscosity, thermal diffusivity and expansion coefficient of air	SI
Rw	Equivalent areal thermal resistance of the kiln wall	m²·K/W
Q̇p, Q̇rec, ΔQ̇kiln	Heat loss rate, recovered heat rate, change in heat drawn from the kiln	W
Ėx	Exergy rate of the heat loss	W
m, cp, τ	Shell mass, specific heat capacity, time constant	kg, J/kg·K, s
φ	Fraction of the shell length covered by the collector	—
Pe, ηII	Convertible electric power; second-law (exergy) efficiency	W, —

REFERENCES

[1]. Çengel, Y. A., Boles, M. A., & Kanoğlu, M. (2024). *Thermodynamics: An engineering approach* (10th ed.). McGraw-Hill Education.

[2]. Cussaguet, P.-M. (2025). *Perspectives du secteur électrique en République démocratique du Congo* [Outlook for the electricity sector in the Democratic Republic of the Congo] (Briefings de l'Ifri). French Institute of International Relations. https://ifri.org/sites/default/files/2025-04/ifri_cussaguet_secteur_electrique_rdc_2025.pdf

[3]. Fierro, J. J., Nieto-Londoño, C., Escudero-Atehortúa, A., Giraldo, M., Jouhara, H., & Wrobel, L. C. (2021). Techno-economic assessment of a rotary kiln shell radiation waste heat recovery system. *Thermal Science and Engineering Progress, 23*, Article 100858. https://doi.org/10.1016/j.tsep.2021.100858

[4]. Kasaeian, A., Afshari, F., Mahmoudkhani, M., Masoumi, A., & Esmaeili Bidhendi, M. (2025). Waste heat recovery by thermodynamic cycles in cement plants: A review. *Energy, 314*, Article 134087. https://doi.org/10.1016/j.energy.2024.134087

[5]. Lienhard V, J. H., & Lienhard IV, J. H. (2024). *A heat transfer textbook* (6th ed., Version 6.00). Phlogiston Press. https://ahtt.mit.edu

[6]. Mahmoud, E. S., Rady, M., Abuhabaya, A. A., & Elsamahy, A. A. (2022). Separate and combined integration of Kalina cycle for waste heat recovery from a cement plant. *Thermal Science, 26*(2), 1907–1925. https://doi.org/10.2298/TSCI210418230M

[7]. Marenco-Porto, C. A., Fierro, J. J., Nieto-Londoño, C., Lopera, L., Escudero-Atehortua, A., Giraldo, M., & Jouhara, H. (2023). Potential savings in the cement industry using waste heat recovery technologies. *Energy, 279*, Article 127810. https://doi.org/10.1016/j.energy.2023.127810

[8]. Mwaba Kalumba, R. (2024). *Étude et dimensionnement d'une centrale thermoélectrique pour l'optimisation de l'énergie thermique émise par le four rotatif : cas de Carrilu S.A.* [Design of a thermoelectric plant for the recovery of heat emitted by a rotary kiln: The case of Carrilu S.A.] [Bachelor's thesis, Institut Supérieur des Techniques Appliquées de Kolwezi].

[9]. Stojić, N., Karamarković, R., Karamarković, M., & Nikolić, M. (2022). Improving design and operating parameters of the recuperator for waste heat recovery from rotary kilns. *Thermal Science, 26*(1), 717–734. https://doi.org/10.2298/TSCI210410239S